



Conformational and solvent effects in structural and spectroscopic properties of 2-hydroxyethyl methacrylate and acrylic acid



Irene Vettori ^{a,b,1}, Marina Macchiagodena ^{a,1}, Marco Pagliai ^{a,*}, Gavino Bassu ^{a,b}, Emiliano Fratini ^{a,b,*}, Piero Baglioni ^{a,b}

^a Department of Chemistry "Ugo Schiff", Via della Lastruccia 3, Sesto Fiorentino (FI), 50019, Italy

^b Consorzio per lo Sviluppo dei Sistemi a Grande Interfase (CSGI), Via della Lastruccia 3, Sesto Fiorentino (FI), 50019, Italy

ARTICLE INFO

Article history:

Received 17 March 2022

Revised 4 May 2022

Accepted 18 May 2022

Available online 23 May 2022

Keywords:

2-hydroxyethyl methacrylate

Acrylic acid

Molecular dynamics simulations

Conformers

Spectroscopic properties

DFT calculations

ABSTRACT

2-hydroxyethyl methacrylate (HEMA) and acrylic acid (AA) are monomers widely used in the production of hydrogels with medium-high water content. The structural and spectroscopic properties of HEMA and AA were studied using a combination of computational strategies based on both density functional theory (DFT) calculations and molecular dynamics (MD) simulations. DFT calculations have confirmed the co-existence of two stable HEMA conformers, while solute-solvent interactions between HEMA and AA with water were characterized by the analysis of MD simulations carried out by employing four different water models and different simulation conditions. The carbonyl and hydroxyl oxygen atoms of HEMA are involved in hydrogen bonding, whereas the ester oxygen atom does not appreciably interacts with the solvent. No significant differences in solute-solvent interactions are found between the two HEMA conformers. Their spectroscopic properties were calculated and the results were compared to experimental data. Although electronic spectra do not really allow a differentiation of the conformers, IR spectra present some peculiar bands to discriminate the presence and obtain information on the ratio of the conformers in solution. To verify the influence of a solvent with higher dipole moment on chemical properties, acetonitrile has been considered as an alternative solvent.

© 2022 Elsevier B.V. All rights reserved.

1. Introduction

2-Hydroxyethyl methacrylate (HEMA) and acrylic acid (AA) are monomers widely used as building blocks in numerous fields of application where the presence of chemical hydrogels with a medium/high water content and good mechanical properties is needed. Their use, both as homopolymers (poly-HEMA and poly-AA) or co-polymers (poly-(HEMA/AA)), spreads from biomedical [1–3] to artworks conservation [4] applications. These monomers deserve deeper investigations for several reasons.

In the case of HEMA, despite the current state of art comprehends several data on the syntheses, characterization and degradation on the polymer (pHEMA) [5–10], just a few papers investigate pHEMA noncovalent inter- and intra-molecular interactions [11–14], and surprisingly, literature lacks even more on studies related to the monomer. Few data report on HEMA

hydrogen bonding from experimental spectra speculations [15,13], proposing dimeric intermolecular or quasi-ring intramolecular structures at low concentration [13]. Both the HEMA carbonyl and alcoholic functional groups appear to be involved in hydrogen bonding, according to vibrational spectra [15,13]. Regarding the monomer structure, as for other methacrylates [16], there are already some experimental evidences of the existence of two stable HEMA conformers in solution, one presenting the carbonyl moiety in *cis* position with respect to the vinyl group, while the other one in *trans* position. In particular, experimental spectra of HEMA present some peaks that can be deconvoluted into contributions arising from these isomers [13]. To the best of our knowledge, the only paper that was entirely devoted to a preliminary study on the HEMA rotational isomers is the one published by Belaidi et al. (2015) [17]. These authors confirmed experimental results with ab-initio calculations and theoretical spectra of the two conformers. However, still some questions to answer remain: (i) what is the percentage of *s-cis*-like conformer with respect to the *s-trans*-like one in solution? (ii) How does this ratio evolve with temperature? (iii) Does this conformation difference affect interactions with the solvent and with other solutes?

* Corresponding author at: Department of Chemistry "Ugo Schiff", Via della Lastruccia 3, Sesto Fiorentino (FI), 50019, Italy (M. Pagliai and E. Fratini).

E-mail addresses: marco.pagliai@unifi.it (M. Pagliai), emiliano.fratini@unifi.it (E. Fratini).

¹ Authors contributed equally.

(iv) How does the presence of these monomeric rotational isomers influence the structure and the properties of HEMA-based polymers?

In the case of AA, for biomedical applications and water treatments, its interactions develop mostly in aqueous environments. For this reason, it is important to analyze the AA monomer behavior in solution to better understand its intermolecular interactions when involved in more complex structures. The pKa of acrylic acid is around 4 [18], thus if we consider almost neutral conditions, AA is present in the deprotonated form (AA^{-1}). As for HEMA, AA can exist in both a *cis*- and a *trans*-like configuration [19,18]. Moreover, *cis*- and *trans*-like AA can combine into *cis-cis* or *trans-trans* or *cis-trans* dimers through hydrogen bonding [19].

The aim of this work is mainly devoted to provide highlights on HEMA and AA conformers in aqueous solution and to describe hydrogen bond interactions with polar solvents. In this respect, the solute-solvent interactions have been studied through MD simulations, employing four different water models [20] to verify the accuracy in hydrogen bond description in different thermodynamic conditions. Molecular dynamics studies on similar systems have been performed elsewhere [21]. The interpretation of the experimental UV-vis and IR spectra of both HEMA and AA in water has been supported by DFT calculations on selected model systems. In addition, the system has been studied in acetonitrile (CH_3CN) to verify the effects on chemical properties of both HEMA and AA of a solvent with higher dipole moment than water.

2. Computational details

2.1. Structural optimization

The molecular structure of the *cis*-like and *trans*-like HEMA conformers and of both the protonated and deprotonated AA was optimized by using ab initio calculations based on Density Functional Theory (DFT) at the B3LYP/6-311++G(d,p) [22–25] level of theory with the Gaussian 09 suite of programs [26]. The torsional energy barrier of the conformers was calculated by scanning the dihedral angle (including the carbonyl and vinyl moieties of each *cis*-like solute) from 0 to 180° with a step-size of 5 degrees. It has been verified that all the optimized minima are characterized by no imaginary vibrational frequencies.

2.2. Force field parameterization

The General AMBER Force Field (GAFF2) parameterization of HEMA and AA molecules (both in its protonated and deprotonated forms) has been obtained by using the PrimaDORAC web interface [27], which provides the topology files for running MD simulations upon a structural input including the molecular charge. While HEMA was considered neutral, AA was investigated both in protonated and deprotonated forms with molecular charge of 0 and −1, respectively.

2.3. Molecular dynamics simulations

MD simulations were performed using GROMACS 2021.2 software [28]. Each single monomer was solvated in a cubic box containing 400 water molecules; subsequent solvations were also performed in CH_3CN lowering the solvent molecules amount to 142; parameterization for CH_3CN was done using GAFF and retrieving atomic charges from elsewhere [29,30]. Four different water models were tested: TIP3P [31], SPC/E [32], TIP3P-FB [33] as three-sites models and TIP4P-FB [33] as four-sites model, respectively; parameters of such water models and application examples can be found elsewhere in literature [34,20]. The initial systems

were minimized by using the steepest descent algorithm, then after an equilibration run of 2 ns, the production run was performed for 10 ns with an integration step of 2 fs. Additional tests, increasing the total simulation time to 50 ns, ensured that no significant differences occur. All simulations were done setting the external pressure at 1 atm using a Parrinello-Rahman Lagrangian [35] with an isotropic stress tensor and keeping constant temperature (at 260, 280 and 298 K, respectively) with a Nosé-Hoover approach [36,37]. In order to study the temperature effect on hydrogen bonding, dynamics with the TIP4P-FB model were also performed at further temperatures (230, 330 and 360 K). Rigid constraints were imposed only on the X-H bonds (with X being any heavy atom) by means of the LINCS algorithm [38]. Electrostatic interactions were treated by using particle-mesh Ewald (PME) [39] method with a grid spacing of 1 Å and a spline interpolation of order 4. Details on MD simulations are also summarized in Table S1. The radial distribution functions, $g(r)$, were calculated with the VMD software [40]. The angle distribution functions, $g(\theta)$, were computed with home made program; the angle θ was defined as the angle between the vectors connecting the donor group (OH) and the donor and the acceptor oxygen atoms ($O \cdots O$). The Spatial Distribution Functions (SDFs) were calculated using TRAVIS software [41,42]. The dihedral angle distributions over the MD simulations at different temperatures were calculated with GROMACS tools. The water self-diffusion coefficient as well as the hydration free energy were also calculated with the GROMACS tools. In particular, the ΔG_{hyd} was calculated using free energy perturbation (FEP) method and using 6 λ values (0.0, 0.2, 0.4, 0.6, 0.8, 1.0) to annihilate charge and Lennard-Jones contributions. Each window was of 2 ns. The Bennett acceptance ratio (BAR) [43] method was used to calculate the free energy differences between the adjacent windows.

2.4. Theoretical spectroscopic characterization

DFT calculations to retrieve the electronic transitions and the vibrational frequencies of each solute were run by the Gaussian 09 suite of programs [26] with the B3LYP/6-311++G(d,p) basis set. Such calculations were done (i) on the single non-solvated molecules (gas phase), (ii) with implicit solvent and (iii) with explicit solvent. For (ii), the Conductor-like Polarizable Continuum Model (C-PCM) [44] was used to describe continuum solvation effects. For (iii), the input consisted in the solute molecule surrounded by the first solvation shell (configuration retrieved by MD) which was embedded in the continuum solvent (C-PCM) to consider further interactions than the first shell one. Explicit solvent molecules corresponded to the ones occurring at virtually 1.8 Å according to the previously calculated $g(r)$ at 298 K.

3. Experimental

3.1. Chemicals

All the following reagents were used without any further purification: HEMA (Sigma Aldrich; assay $\geq 98\%$), AA (Fluka; assay $\geq 99.0\%$), sodium hydroxyde (NaOH; Sigma Aldrich; assay $\geq 98\%$); deuterium oxide (D_2O ; Eurisotop; assay $\geq 99.90\%$); CH_3CN (Sigma Aldrich; assay $\geq 99.8\%$).

3.2. Experimental spectroscopic characterization

Experimental UV-vis and IR spectra of HEMA and AA solutions were recorded. Solutions were prepared both in D_2O and CH_3CN media, ranging from 0.001 to 1 M. Small amounts of NaOH were added to the deuterated solutions to keep a strongly basic environ-

ment (i.e. $\text{pH} \geq 10$). Absorption spectra were recorded by a Cary 60 UV-vis spectrophotometer, scanning wavelengths from 190 to 400 nm at 0.5 nm steps with a scan rate of 500 nm/min. Vibrational spectra were obtained by a Thermo Nicolet Nexus 870 spectrometer equipped with an MCT detector, recording 128 scans at 4 cm^{-1} resolution in the $4000\text{--}650 \text{ cm}^{-1}$ range.

4. Results and discussion

4.1. Torsional energy barrier

As shown in Fig. 1, the torsional energy barrier between the isolated *cis*- and the *trans*-like HEMA conformers corresponds to about 4.7 kcal/mol. The energy barrier does not allow the inter-conversion of one conformer in the other at room temperature. Considering the main solvent effects through an implicit solvent (i.e. water or CH_3CN), the switching between the two conformers results slightly easier, as the torsional energy barrier results lowered to 4.0 kcal/mol. The energy barrier is expected to be higher in solution than in gas phase if an explicit solvent, and thus hydrogen bonding, is considered. The *trans*-like conformer results to be slightly more stable than the *cis*-like one in gaseous phase ($\Delta E_{\text{trans-cis}}$ equal to 0.263 kcal/mol), while their become more similar in solution when considering an implicit solvent ($\Delta E_{\text{trans-cis}}$ equal to -0.132 kcal/mol both for water and acetonitrile) and essentially the same adding an explicit solvent ($\Delta E_{\text{trans-cis}}$ equal to 0.010 kcal/mol for deuterated water). The energy values of the

conformers with explicit solvent were retrieved from calculations with the Gaussian tool.

The distribution of the dihedral angle for the two HEMA conformers has been evaluated by analysing the trajectories of MD simulations, confirming their stability. Indeed, as it is shown in Fig. 2 the dihedral angle C1-C2-C3-O4 (for labeling see inset of Fig. 1) populates the corresponding energy minima, which are located at 0° for the *cis*-like and at 180° for *trans*-like conformer, respectively. The dihedral angle C1-C2-C3-O4 distribution of *cis*-like conformer was calculated for all the MD simulations (230, 260, 280, 298, 330 e 360 K) to investigate the effect of temperature. A broader distribution always peaked at 0° is obtained at higher temperature confirming the conformer stability (see Figure S1 in ESI), also when the system is simulated at temperatures different from standard conditions.

Protonated AA results to be more stable in its *cis*-like form both in gaseous and in liquid state (see Fig. 1), as reported in the work of Kulbida et al. [45]. The torsional energy barrier results to be lower if implicit solvents (i.e. water or CH_3CN) are considered. The deprotonated AA presents lower torsional energy barrier than the protonated one, possibly as a result of the electronic delocalization present in the carboxylate anion.

4.2. Solute-solvent interactions

The *cis*- and *trans*-like HEMA conformers present similar $g(r)$ (see Fig. 3) and $g(\theta)$ (see Figure S2), meaning that the interactions with the water do not really change. As depicted in Fig. 3 by the first maximum, the main solute-solvent interactions are given by the carbonyl, C=O (Oc), and the hydroxy, C-O-H (Oa, Ha), groups (see panels a, c and d of the figure). Vice versa, the alkoxy C-O-R (Oe) moiety almost does not take part to hydrogen bonding with hydrogen atoms of water (Hw). Considering the $g(r)$ obtained with the TIP4P-FB model at room T, the maximum probability to find water solvating HEMA is at 1.8 \AA for both C=O and C-O-H groups in HEMA. As shown by the integrals computed at the first $g(r)$ minimum reported in Fig. 3, the first solvation shell extending to $\sim 2.5 \text{ \AA}$ includes about two water molecules around the carbonyl group (see panel (a)) and about three water molecules around the hydroxyl moiety (see panels (c) and (d)), both in donor (~ 1) and acceptor (~ 2) fashions. The 3D graphical representations of SDFs confirm the $g(r)$ results (see Fig. 4), corroborating the presence of hydrogen bonds. Although the isovalue adopted to show the results are not the same, it is possible to visualize the acceptor/donor character of the two groups and also to appreciate the hydrogen bond directionality. The $g(\theta)$ (see Figure S2) confirms the directional character of hydrogen bond interactions as expected: all the functions drop down after virtually 20° and go to zero around 45° . The only exception is found for the $g(\theta)_{\text{Hw} \dots \text{Oe}}$ function, and such behaviour is correlated to the extremely weak interaction given by the ester group. When lowering the temperature, hydrogen bonding seems to become more directional (i.e. narrower $g(r)$) both with the carbonyl and the hydroxyl moiety as shown by Fig. 5 showing the radial distribution function between donor-acceptor groups calculated during MD simulations of *cis*-like HEMA conformer in TIP4P-FB water at several temperatures (230, 260, 280, 298, 330 and 360 K). When the system is simulated at 360 K, the distribution of water molecules looks more disordered (panel (d) of the figure). This is consistent with the increased molecular motion in solution as a consequence of the greater thermal agitation induced by the temperature change.

The ΔG_{hyd} obtained for HEMA is $-6.4 \pm 0.6 \text{ kcal/mol}$; this results is in agreement with that determined in other studies [46]. Such value confirms the favorable interaction of HEMA with water.

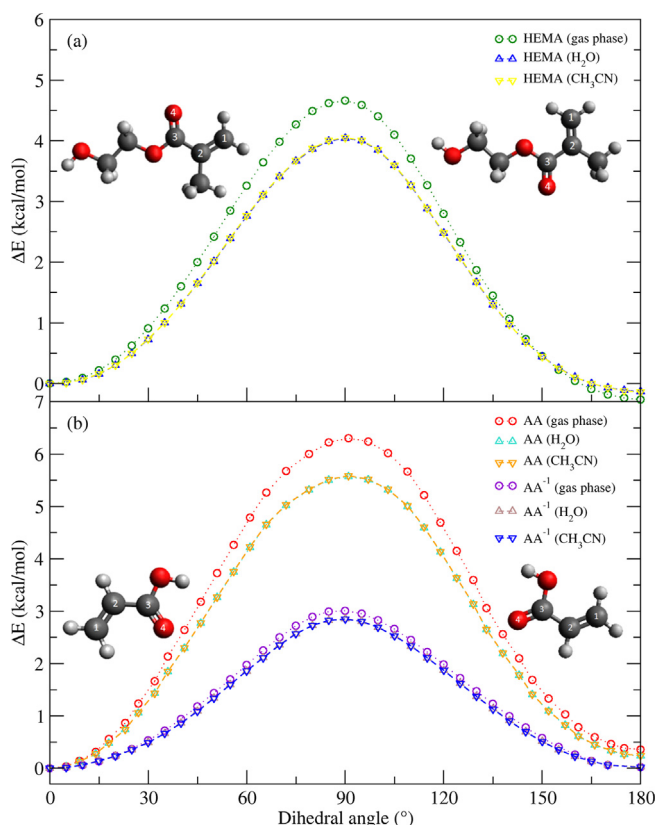


Fig. 1. Potential energy profile of (a) C1-C2-C3-O4 HEMA dihedral angle calculated in the gas phase (green), in water (blue), in CH_3CN (yellow) and (b) C1-C2-C3-O4 AA dihedral angle in its protonated (gas phase (red), in water (cyan) and in CH_3CN (orange)) and deprotonated (gas phase (violet), in water (brown) and in CH_3CN (blue)) form. The solvent effect is taken into account by using the C-PCM approach. The atom labelling is reported on the ball-and-stick models in the insets of the figure.

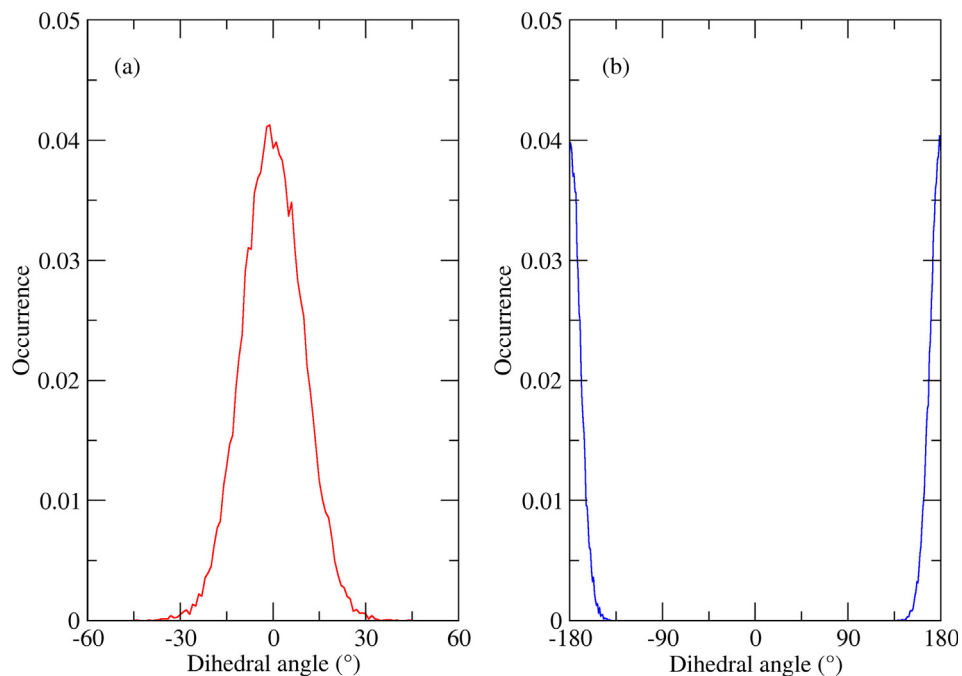


Fig. 2. C1-C2-C3-O4 dihedral angle distribution calculated during the 10 ns MD simulations of (a) cis-like and (b) trans-like HEMA conformers obtained in the case of TIP4P-FB water model.

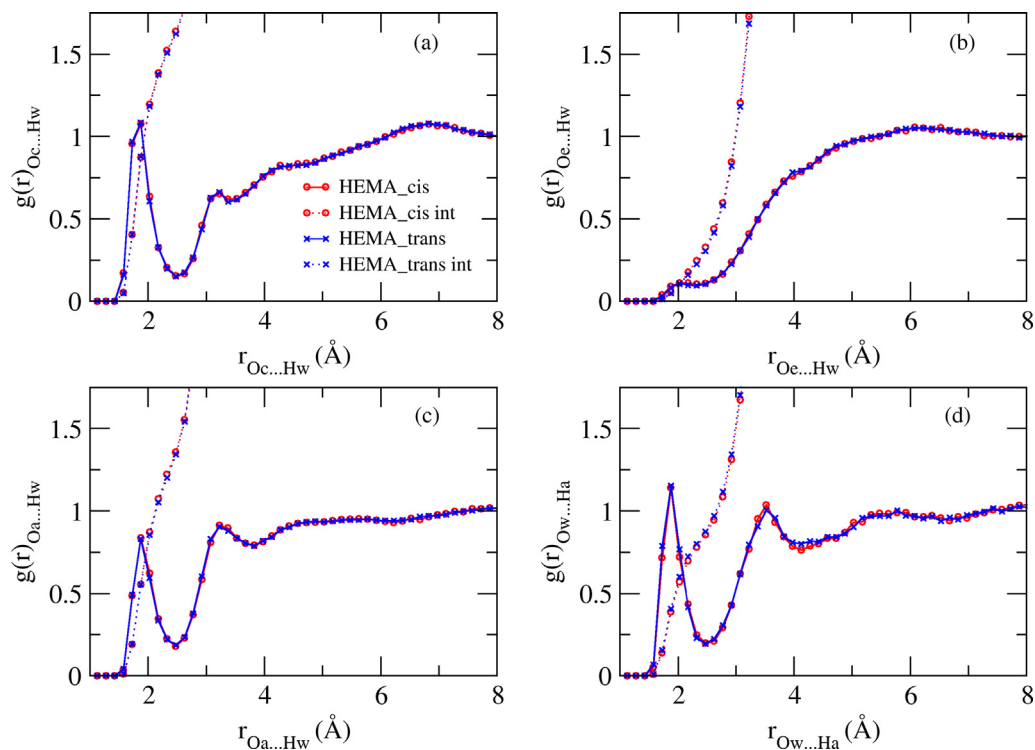


Fig. 3. Radial distribution functions (continuous lines) and their integral forms (dashed lines) for cis- and trans-like HEMA conformers at 298 K with the TIP4P-FB water model. The $g(r)$ considers (a) the carbonyl oxygen atom (Oc) and the water hydrogen atoms (Hw); (b) the alkoxy oxygen atom (Oe) and the water hydrogen atoms; (c) the hydroxyl oxygen atom (Oa) and the water hydrogen atoms; (d) the water oxygen atom (Ow) and the hydroxyl hydrogen atom (Ha).

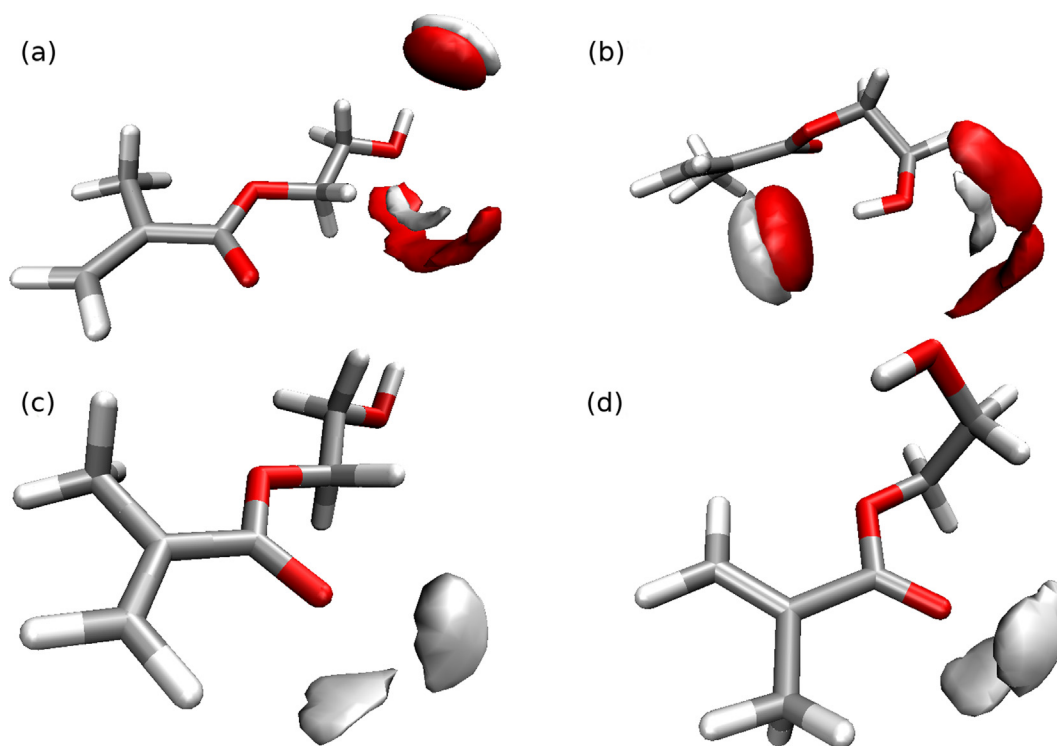


Fig. 4. Spatial distribution functions of the water hydrogen atom (white) and water oxygen atom (red) around (a) alcoholic moiety of *cis*-like HEMA, (b) alcoholic moiety of *trans*-like HEMA, (c) carbonyl moiety of *cis*-like HEMA and (d) carbonyl moiety of *trans*-like HEMA. In (a) and (b) are shown at an isovalue of 75 nm^{-3} , in (c) and (d) at 65 nm^{-3} .

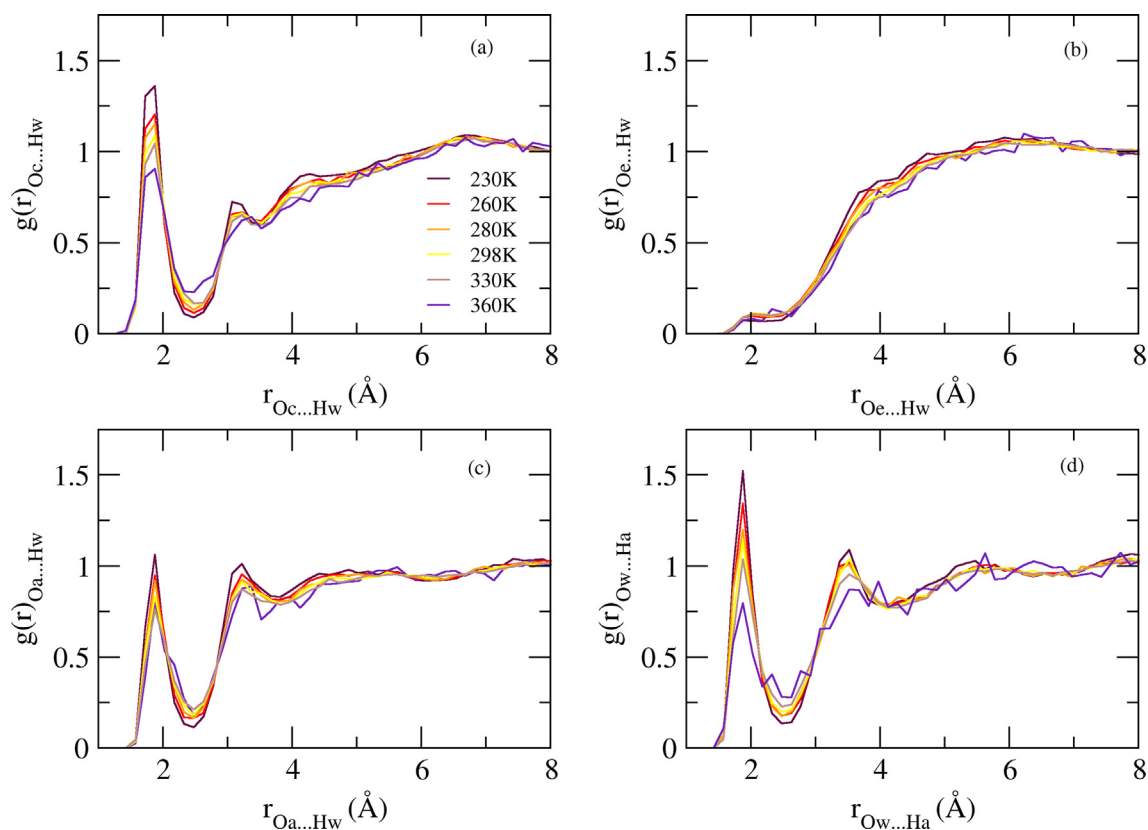


Fig. 5. Radial distribution functions of the *cis*-like HEMA conformers at different T with the TIP4P-FB water model. The $g(r)$ considers (a) the carbonyl oxygen atom (Oc) and the water hydrogen atoms (Hw); (b) the alkoxy oxygen atom (Oe) and the water hydrogen atoms; (c) the hydroxyl oxygen atom (Oa) and the water hydrogen atoms; (d) the water oxygen atom (Ow) and the hydroxyl hydrogen atom (Ha).

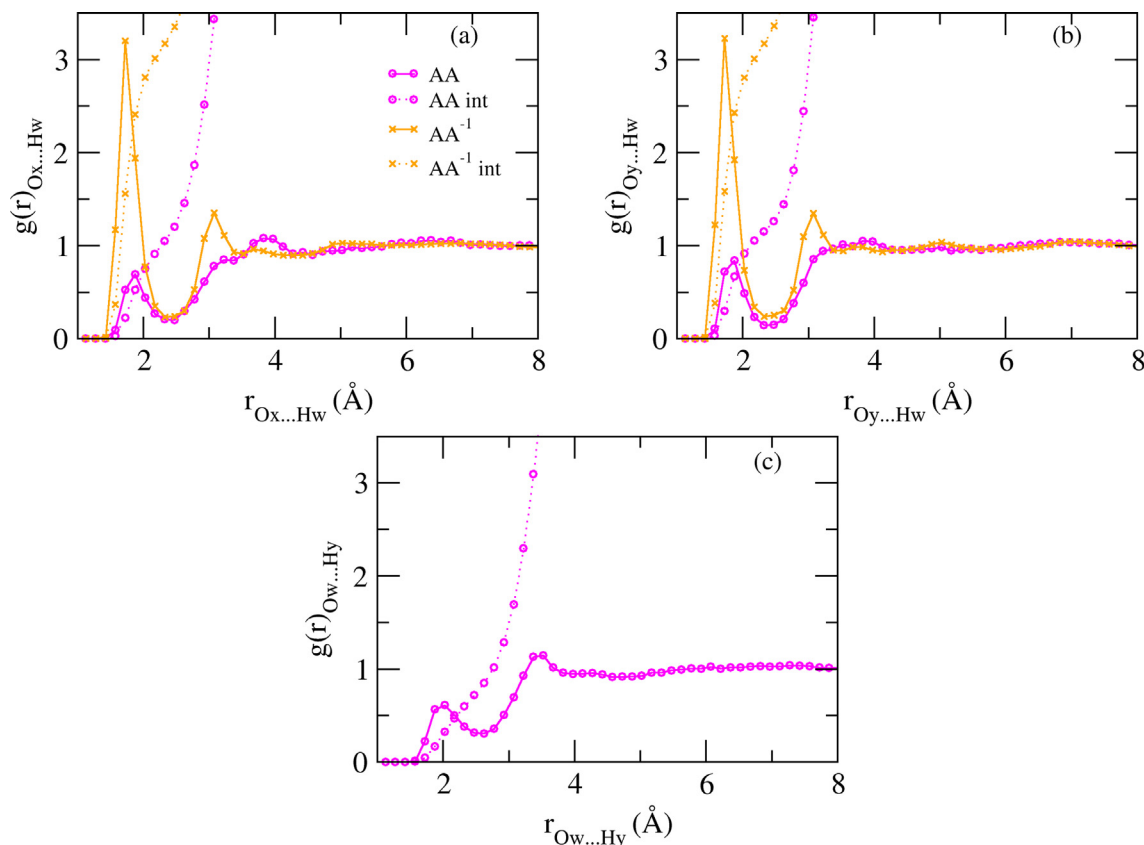


Fig. 6. Radial distribution functions (continuous lines) and their integrals (dashed lines) for AA in its protonated and deprotonated forms. The $g(r)$ considers (a) the carbonyl oxygen atom (Ox) and the water hydrogen atoms (Hw); (b) the hydroxyl (Oy) oxygen atom and the water hydrogen atoms (Hw) and (c) the water oxygen atom (Ow) and the hydroxyl hydrogen atom (Hy).

In the case of AA, both the carboxylic oxygen atoms (i.e. carbonyl, Ox and hydroxyl, Oy) take part to hydrogen bonding. As for HEMA, according to the $g(r)$, water molecules are most likely to occur at 1.8 Å far from the AA oxygen atoms (see Fig. 6). AA $g(r)$ integrals are quite different with respect to HEMA ones instead: the first solvation shell of AA in its protonated form includes four water molecules around the carboxyl moiety, while integrals of deprotonated AA show that the first solvation shell is composed by six water molecules in total, half around each AA oxygen (Ox and Oy). When the AA is in the protonated form, the hydroxyl group also plays the role of hydrogen bond donor as shown in Fig. 6 (see panel (c)). The $g(\theta)$ confirms the hydrogen bond directional character also in the case of AA (see Figure S3). The ΔG_{hyd} obtained for AA is -5.45 ± 0.07 kcal/mol; this value is consistent with experimental ΔG_{hyd} of species with similar structure [47].

The water self-diffusion coefficients, calculated on the systems with the TIP4P-FB model, are in line with bulk water ones while varying temperature (i.e. system density, calculated for cis-like HEMA in TIP4P-FB at T 298 K, is equal to $1.92 \pm 0.09 \cdot 10^{-5}$ cm²/s), as the solvent amount is huge compared to just one molecule of solute in the systems [48,49]. Results are reported in Table S2.

Different water models (i.e. TIP3P, SPC/E, TIP3P-FB and TIP4P-FB) have been used to study cis-like HEMA conformer and AA and sort out their effect on the system solvation description. Changing water model does not deeply affect the $g(r)$ at room T for either solutes, while differences become more important as T is lowered. The water model that best fits the hydrogen bonding description (see Fig. 7 and Figure S4) is TIP4P-FB, that differently

for the other models (Figure S4) can reproduce the structural properties even at low T (see Table 1). In these simulations, the expected density values are close to the density of bulk water as a result of the very low concentration of the solutes (i.e. only one solute molecule is considered). Graphs and tables with experimental bulk water density versus calculated values are reported elsewhere and can be used for comparison [33,50,51]. The water models considered in this study reproduce the effect of T on the density with the highest value encountered at 280 K. Less accuracy is encountered in the case of SPC/E.

To obtain further insights on the structural, dynamic and spectroscopic properties of both HEMA and AA, MD simulations have been carried out also in acetonitrile. This choice allows to verify the influence of an aprotic solvent but with higher dipole moment than water on the structural properties of the investigated systems. In CH₃CN solution, HEMA carbonyl oxygen, C=O (Oc) still interacts with solvent hydrogen atoms though the interaction is at higher distance values and the $g(r)$ peak is broader (see panel (a) in Figure S5). Furthermore, the HEMA hydrogen bond donor character becomes less pronounced in CH₃CN, indeed although the first peak of $g(r)_{\text{N} \cdots \text{Ha}}$ is still present (see panel (d) in Figure S5), the integral value calculated at the first minimum is lower. The HEMA in CH₃CN prefers to form an intramolecular hydrogen bond between the hydroxyl hydrogen atom (Ha) and the carbonyl oxygen atom (Ox) obtaining an almost cyclic structure. A similar result has been found analyzing the radial distribution functions between AA (in protonated and deprotonated form) and CH₃CN: both the carboxylic oxygen atoms (i.e. carbonyl, Ox and hydroxyl, Oy) take part in weaker hydrogen bonds with broader $g(r)$ peaks shifted at

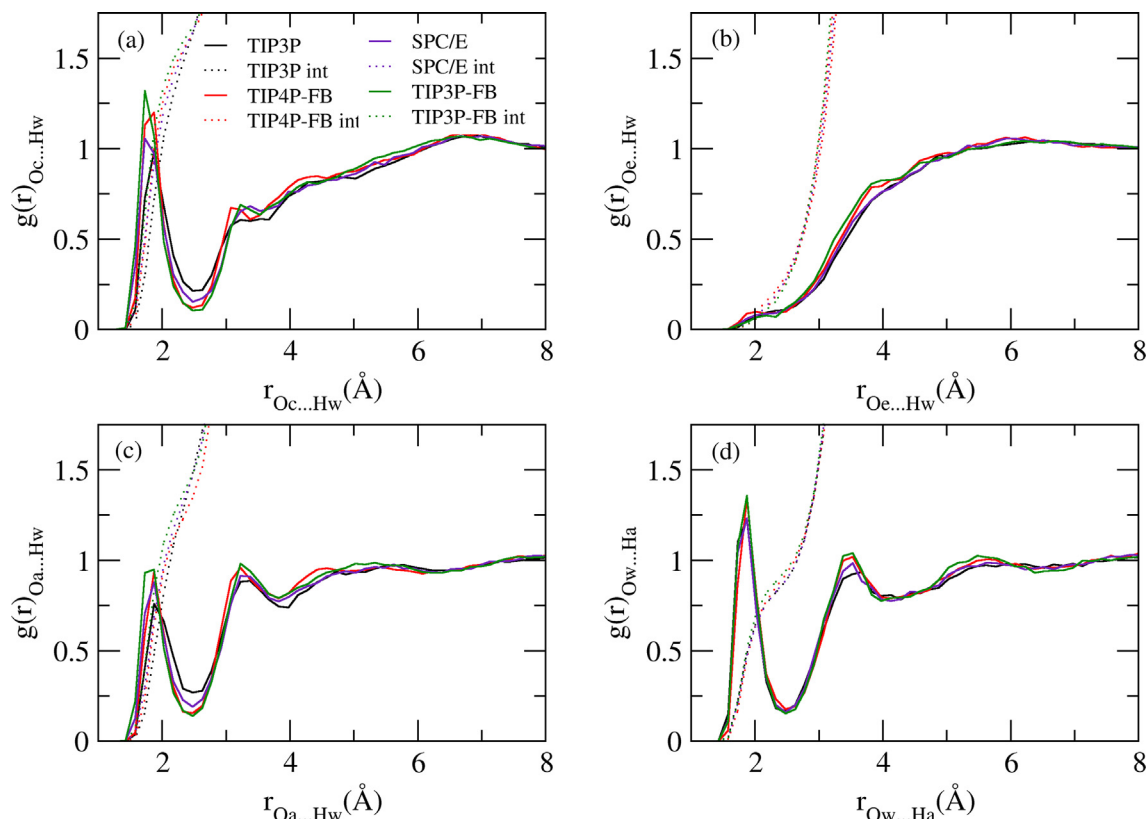


Fig. 7. Radial distribution functions (continuous lines) and their integrals (dashed lines) for the *cis*-like HEMA conformer at 260 K. The $g(r)$ considers (a) the carbonyl oxygen atom (Oc) and the water hydrogen atoms (Hw); (b) the alkoxy oxygen atom (Oe) and the water hydrogen atoms; (c) the hydroxyl oxygen atom (Oa) and the water hydrogen atoms; (d) the water oxygen atom (Ow) and the hydroxyl hydrogen atom (Ha).

Table 1

Calculated densities from MD simulations of *cis*-like HEMA conformer and protonated AA solvated using the different water models and at different temperatures.

Density (kg/m ³)			
<i>cis</i> -like HEMA conformer			
	260 K	280 K	298 K
TIP3P	987.4 ± 0.1	1002.4 ± 0.1	987.1 ± 0.2
TIP3P-FB	1007.2 ± 0.5	1003.9 ± 0.2	997.7 ± 0.1
SPC/E	1000.7 ± 0.1	1008.9 ± 0.1	1000.6 ± 0.2
TIP4P-FB	1000.3 ± 0.5	1001.9 ± 0.2	998.8 ± 0.2
protonated AA			
	260 K	280 K	298 K
TIP3P	987.5 ± 0.1	1002.3 ± 0.2	987.1 ± 0.1
TIP3P-FB	997.1 ± 0.2	1003.1 ± 0.2	997.2 ± 0.2
SPC/E	1014.0 ± 0.3	1008.6 ± 0.1	1000.6 ± 0.1
TIP4P-FB	999.2 ± 0.3	1001.2 ± 0.1	998.5 ± 0.2

higher distance values (Figure S6). The hydrogen bond donor character of protonated AA in CH₃CN does not change and it is the same found in water.

4.3. Spectroscopic characterization

The experimental UV–vis absorption spectrum of HEMA in D₂O (Fig. 8) presents a maximum around 195 nm (the peak is shifted to 205 nm in CH₃CN, see Figure S7). The calculated electronic transitions of the *cis*- and *trans*-like HEMA molecules are extremely similar. Considering the UV–vis spectra of the non-solvated conformers, the *cis*-like one is virtually 5 nm red-shifted with

respect to the *trans*-like one, while adding an implicit solvent (with C-PCM) the difference is around 10 nm. Improvements in the calculated band description with respect to the experimental one arise when using an explicit solvent coupled to C-PCM. We consider the first solvation shell together with C-PCM explicitly, differences between the bands of the two conformers disappear completely (see panel (c) of Fig. 8). Thus, UV–vis spectroscopy does not really allow to discriminate between the two conformers.

By comparing the vibrational frequencies of the two conformers, differences become much more evident (see Fig. 9). The experimental IR band corresponding to the carbonyl stretching mode of HEMA in D₂O (around 1700 cm⁻¹) is of particular interest because of its asymmetric shape, which is expected to be fitted by the distinct bands of the two conformers. The simulated IR spectra of the non-solvated *cis*-like and *trans*-like forms present the C=O stretching mode shifted to 1773 and 1764 cm⁻¹, respectively. It is thus necessary to introduce a solvent description for better fitting the experimental data. When introducing implicit water, the *cis*-like peak is shifted to 1729 cm⁻¹ and the *trans*-like one to 1721 cm⁻¹. Such shift is further corrected by adding explicitly five deuterated water molecules, belonging to the first solvation shell, coupled to the C-PCM model. In fact, by using this combined approach, the carbonyl stretching band of the *cis*-like conformer occurs at 1702 cm⁻¹, while the *trans*-like one at 1694 cm⁻¹ [52]. Comparing the carbonyl stretching band intensities, the ratio of *trans*- to *cis*-like HEMA conformers results to be almost 56.5: 43.5.

The experimental HEMA carbonyl stretching band in CH₃CN is at virtually 1718 cm⁻¹, and in this case the band shape is symmetric (see Figure S8). The simulated vibrational bands of the *cis*- and *trans*-like HEMA conformers with implicit CH₃CN nearly overlap at

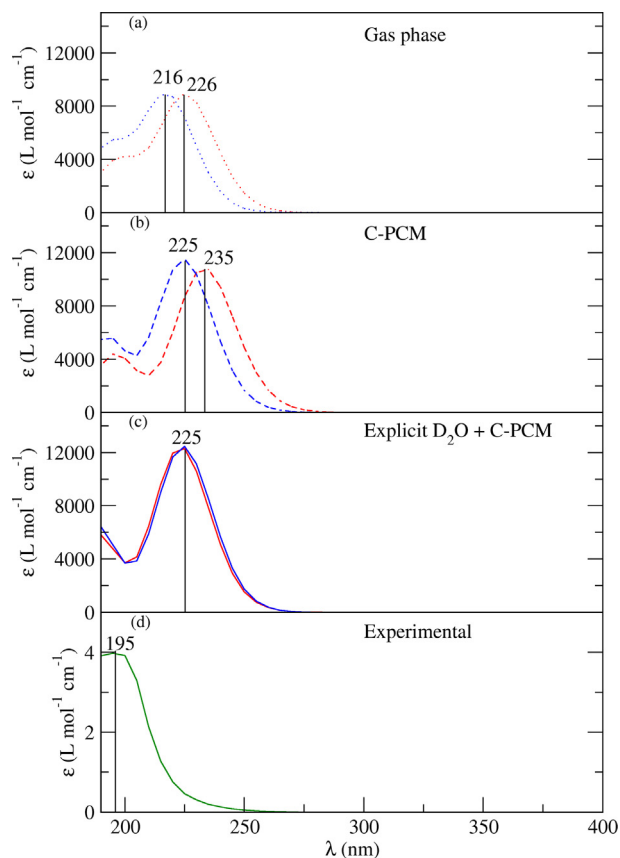


Fig. 8. Calculated *cis*-like (red lines) and *trans*-like (blue lines) HEMA conformers UV-vis spectra (a) in gas phase, (b) with C-PCM, (c) with explicit solvent + C-PCM and (d) experimental HEMA UV-vis spectrum in D₂O.

1730 and 1721 cm⁻¹, respectively (see Figure S8). Because of the extremely similar calculated energies of the *cis*- and *trans*-like HEMA conformers (considering calculations with implicit CH₃CN), we can exclude the presence of just one conformer and hypothesize that both the conformers are present in almost 1:1 ratio and that both the corresponding bands can be convoluted into the experimental one.

As expected, AA is present in its deprotonated form when the acid is exposed to strongly basic conditions. Its experimental UV-vis spectrum presents an electronic band at 195 nm; such band is almost perfectly fitted by the calculated one at 201 nm considering explicit D₂O + C-PCM (see Figure S9). The experimental UV-vis spectrum of AA in CH₃CN presents a band in which both the protonated and the deprotonated species can fit (see Figure S10). By comparing the experimental vibrational spectrum of AA in D₂O and the simulated one with explicit solvent + C-PCM (see Figure S11), the calculated band at 1249 cm⁻¹ fits the experimental one at 1205 cm⁻¹, corresponding to the C-O asymmetric stretching mode [53]. Again, the best agreement between calculated and experimental data arises from the introduction of explicit solvent molecules. Vice versa, in the experimental IR spectrum of AA in CH₃CN (without pH corrections) bands corresponding to both protonated and deprotonated AA are present (see Figure S12).

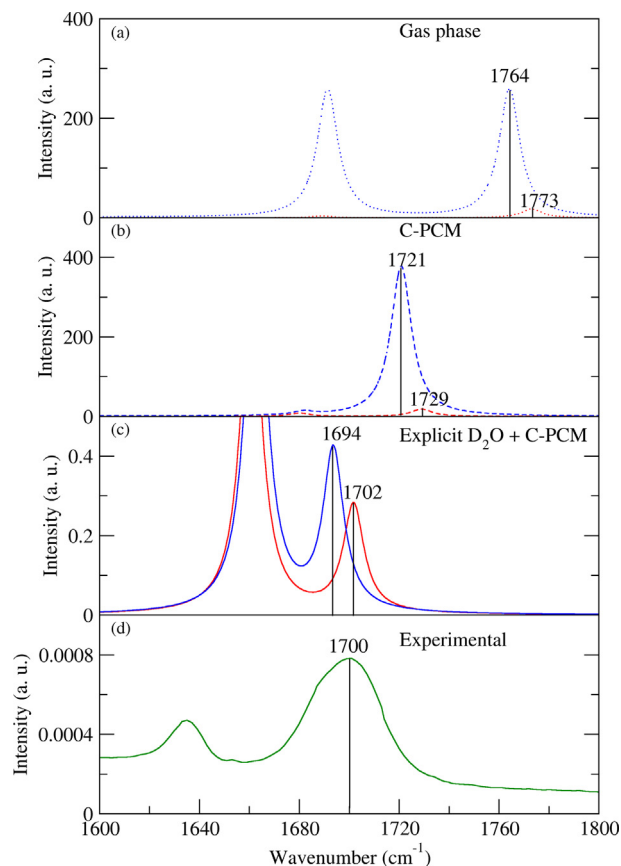


Fig. 9. Calculated *cis*-like (red lines) and *trans*-like (blue lines) HEMA conformers C=O stretching IR bands (a) in gas phase, (b) with C-PCM, (c) with explicit solvent + C-PCM and experimental HEMA IR spectrum in D₂O.

5. Conclusions

The co-existence of two stable HEMA conformers in solution was confirmed by both experimental and theoretical results. The *cis*-like protonated AA is confirmed to be more stable than the *trans*-like form. Solute-solvent interactions are equal for both conformers, and they occur mainly through the carbonyl and alcoholic moieties in HEMA and through the carboxylic group in AA, both in donor and acceptor fashions. Switching from water to CH₃CN as solvent, the probability to find a hydrogen bond network between HEMA or AA and the solvent itself gets lower. Moreover, when present, solute-solvent hydrogen bonding with CH₃CN is weaker. The hydrogen bonding description far changes when switching from water to CH₃CN as solvent, resulting negligible for both HEMA and AA: when comparing *g*(*r*) of systems in water to systems in acetonitrile, there are several differences in the plotted curves concerning (i) the first maximum position (related to hydrogen bond strength), height (related to probability) and width (related to directionality), (ii) the integral corresponding to the first minimum (regarding hydrogen bonds amount), (iii) further solvation shells description. A reason for such differences can be the major polarity of water compared to CH₃CN. The usage of explicit solvent molecules coupled to C-PCM improves the description of calculated spectra for both HEMA and AA monomers. Electronic transitions

do not allow to discriminate between the *cis*-like and *trans*-like HEMA conformers, while vibrational ones do. In particular, the HEMA carbonyl stretching band suggests a different ratio of the *trans*- and *cis*-like HEMA conformers in solution, which was calculated to be 56.5: 43.5 at ambient conditions by considering their dipole moments. Such difference could influence HEMA-containing polymeric structures, especially in case of polymerization at low T, and will therefore be considered in further studies for longer HEMA chains.

Declaration of Competing Interest

The authors declare that they have no known competing financial interests or personal relationships that could have appeared to influence the work reported in this paper.

Acknowledgments

Authors acknowledge “Progetto Dipartimenti di Eccellenza 2018–2022” allocated to Department of Chemistry “Ugo Schiff”, MUR PRIN-2017249YEF and Consorzio Interuniversitario per lo Sviluppo dei Sistemi a Grande Interfase, CSGI (Center for Colloid and Surface Science) for the financial support.

Appendix A. Supplementary material

Supplementary data associated with this article can be found, in the online version, at <https://doi.org/10.1016/j.molliq.2022.119428>.

References

- [1] E. De Giglio, D. Cafagna, M.M. Giangregorio, M. Domingos, M. Mattioli-Belmonte, S. Cometa, PHEMA-based thin hydrogel films for biomedical applications, *J. Bioact. Compat. Polym.* 26 (2011) 420–434. <https://doi.org/10.1177/0883911511410460>.
- [2] S.S. Halacheva, D.J. Adlam, E.K. Hendow, T.J. Freemont, J. Hoyland, B.R. Saunders, Injectable biocompatible and biodegradable pH-responsive hollow particle gels containing poly(acrylic acid): The effect of copolymer composition on gel properties, *Biomacromolecules* 15 (2014) 1814–1827. <https://doi.org/10.1021/bm5002069>.
- [3] X. Jin, Y.-L. Hsieh, pH-responsive swelling behavior of poly(vinyl alcohol)/poly(acrylic acid), *Polymer* 46 (2005) 5149–5160. <https://doi.org/10.1016/j.polymer.2005.04.066>.
- [4] J.A.L. Domingues, N. Bonelli, R. Giorgi, E. Fratini, F. Gorel, P. Baglioni, Innovative hydrogels based on semi-interpenetrating p(hema)/pvp networks for the cleaning of water-sensitive cultural heritage artifacts, *Langmuir* 29 (2013) 2746–2755. <https://doi.org/10.1021/la3048664>.
- [5] L. Ferreira, M.M. Vidal, M.H. Gil, Evaluation of poly(2-hydroxyethyl methacrylate) gels as drug delivery systems at different pH values, *Int. J. Pharm.* 194 (2000) 169–180. [https://doi.org/10.1016/S0378-5173\(99\)00375-0](https://doi.org/10.1016/S0378-5173(99)00375-0).
- [6] J.R. Meakin, D.W.L. Hukins, Thermal analysis of poly(2-hydroxyethyl methacrylate)(pHEMA) hydrogels, *J. Mater. Sci.: Mater. Med.* 14 (2003) 9–15. <https://doi.org/10.1023/A:1021589017753>.
- [7] E. Vargün, A. Usanmaz, Degradation of poly(2-hydroxyethyl methacrylate) obtained by radiation in aqueous solution, *J. Macromol. Sci. - Pure Appl. Chem.* 47 (2010) 882–891. <https://doi.org/10.1080/10601325.2010.501304>.
- [8] M.F. Passos, D.R.C. Dias, G.N.T. Bastos, A.L. Jardini, A.C.B. Benatti, C.G.B.T. Dias, R. Maciel Filho, pHEMA hydrogels, *J. Therm. Anal. Calorim.* 125 (2016) 361–368. <https://doi.org/10.1007/s10973-016-5329-6>.
- [9] H. Ayhan, F. Ayhan, Water based pHEMA hydrogels for controlled drug delivery, *Turkish J. Biochem.* 43 (3) (2018) 228–239. <https://doi.org/10.1515/tjb-2017-0250>.
- [10] M. Lee, J. Lee, J. Jang, C. Nah, Y. Huh, Fabrication and characterization of modified poly(2-hydroxyethyl methacrylate)(pHEMA) hydrogels by thermal/photo polymerization, *Elastom. Compos.* 54 (4) (2019) 359–367. <https://doi.org/10.7473/EC.2019.54.4.359>.
- [11] M.F. Refojo, Hydrophobic interaction in poly(2-hydroxyethyl methacrylate) homogeneous hydrogel, *J. Polym. Sci. Part A: Polym. Chem.* 5 (12) (1967) 3103–3113. <https://doi.org/10.1002/pol.1967.150051211>.
- [12] J.-T. Kim, M.-J. Lee, U.-R. Kim, M. Kimura, Y. Aoki, A. Imamura, Theoretical synthesis of poly-(2-hydroxyethylmethacrylate) by uniform localization of molecular orbitals calculation, *J. Polym. Sci. Part A: Polym. Chem.* 39 (15) (2001) 2677–2682. <https://doi.org/10.1002/pola.1244>.
- [13] S. Morita, K. Kitagawa, Y. Ozaki, Hydrogen-bond structures in poly(2-hydroxyethyl methacrylate): Infrared spectroscopy and quantum chemical calculations with model compounds, *Vib. Spectrosc.* 51 (1) (2009) 28–33. <https://doi.org/10.1016/j.vibspec.2008.09.008>.
- [14] S. Morita, Hydrogen-bonds structure in poly(2-hydroxyethyl methacrylate) studied by temperature-dependent infrared spectroscopy, *Front. Chem.* 2 (2014) 10. <https://doi.org/10.3389/fchem.2014.00010>.
- [15] M.T. Lemon, M.S. Jones, J.W. Stansbury, Hydrogen bonding interactions in methacrylate monomers and polymers, *J. Biomed. Mater. Res. A* 83A (3) (2007) 734–746. <https://doi.org/10.1002/jbm.a.31448>.
- [16] O. Belaidi, T. Bouchaour, U. Maschke, Am 1 and dft: Conformational and vibrational spectra analysis of butyl methacrylate, *Int. J. Chem. Anal. Sci.* 4 (4) (2013) 185–196. <https://doi.org/10.1016/j.ijcas.2013.08.001>.
- [17] O. Belaidi, M. Adjim, T. Bouchaour, U. Maschke, Ft-ir and ft-raman spectra of 2-hydroxyethyl methacrylate – a conformational and vibrational analysis, *Spectrochim. Acta A Mol. Biomol. Spectrosc.* 148 (2015) 396–404. <https://doi.org/10.1016/j.saa.2015.03.101>.
- [18] E.L. Ibarra-Montaño, N. Rodríguez-Laguna, A. Sánchez-Hernández, A. Rojas-Hernández, Determination of pKa values for acrylic, methacrylic and itaconic acids by ¹H and ¹³C nmr in deuterated water, *J. Appl. Sol. Chem.* 4 (1) (2015) 7–18. <https://doi.org/10.6000/1929-5030.2015.04.01.2>.
- [19] J. Umemura, S. Hayashi, Infrared spectra and molecular configurations of liquid and crystalline acrylic acids, *Bull. Inst. Chem. Res.* 52 (4) (1975) 585–595.
- [20] M. Pagliai, M. Macchiagodena, P. Procacci, G. Cardini, Evidence of a low-high density turning point in liquid water at ordinary temperature under pressure: A molecular dynamics study, *J. Phys. Chem. Lett.* 10 (20) (2019) 6414–6418. <https://doi.org/10.1021/acs.jpclett.9b02724>.
- [21] Y. Liu, Y. Zhang, B. Ren, Y. Sun, Y. He, F. Cheng, J. Xu, J. Zheng, Molecular dynamics simulation of the effect of carbon space lengths on the antifouling properties of hydroxyalkyl acrylamides, *Langmuir* 35 (9) (2019) 3576–3584. <https://doi.org/10.1021/acs.langmuir.8b04229>.
- [22] A.D. Becke, Density-functional thermochemistry. iii. the role of exact exchange, *J. Chem. Phys.* 98 (7) (1993) 5648–5652. <https://doi.org/10.1063/1.464913>.
- [23] C. Lee, W. Yang, R.G. Parr, Development of the Colle-Salvetti correlation-energy formula into a functional of the electron density, *Phys. Rev. B* 37 (1988) 785–789. <https://doi.org/10.1103/PhysRevB.37.785>.
- [24] S.H. Vosko, L. Wilk, M. Nusair, Accurate spin-dependent electron liquid correlation energies for local spin density calculations: a critical analysis, *Can. J. Phys.* 58 (8) (1980) 1200–1211. <https://doi.org/10.1139/p80-159>.
- [25] P.J. Stephens, F.J. Devlin, C.F. Chabalowski, M.J. Frisch, Ab initio calculation of vibrational absorption and circular dichroism spectra using density functional force fields, *J. Phys. Chem.* 98 (45) (1994) 11623–11627. <https://doi.org/10.1021/j100096a001>.
- [26] M.J. Frisch, G.W. Trucks, H.B. Schlegel, G.E. Scuseria, M.A. Robb, J.R. Cheeseman, G. Scalmani, V. Barone, B. Mennucci, G.A. Petersson, H. Nakatsuji, M. Caricato, X. Li, H.P. Hratchian, A.F. Izmaylov, J. Bloino, G. Zheng, J.L. Sonnenberg, M. Hada, M. Ehara, K. Toyota, R. Fukuda, J. Hasegawa, M. Ishida, T. Nakajima, Y. Honda, O. Kitao, H. Nakai, T. Vreven, J.A. Montgomery, Jr., J.E. Peralta, F. Ogliaro, M. Bearpark, J.J. Heyd, E. Brothers, K.N. Kudin, V.N. Staroverov, R. Kobayashi, J. Normand, K. Raghavachari, A. Rendell, J.C. Burant, S.S. Iyengar, J. Tomasi, M. Cossi, N. Rega, J.M. Millam, M. Klene, J.E. Knox, J.B. Cross, V. Bakken, C. Adamo, J. Jaramillo, R. Gomperts, R.E. Stratmann, O. Yazyev, A.J. Austin, R. Cammi, C. Pomelli, J.W. Ochterski, R.L. Martin, K. Morokuma, V.G. Zakrzewski, G.A. Voth, P. Salvador, J.J. Dannenberg, S. Dapprich, A.D. Daniels, O. Farkas, J.B. Foresman, J.V. Ortiz, J. Cioslowski, D.J. Fox, Gaussian Development Version Revision H.38, gaussian Inc., Wallingford CT, 2009.
- [27] P. Procacci, Primadorac: A free web interface for the assignment of partial charges, chemical topology, and bonded parameters in organic or drug molecules, *J. Chem. Inf. Model.* 57 (6) (2017) 1240–1245. <https://doi.org/10.1021/acs.jcim.7b00145>.
- [28] M.J. Abraham, T. Murtola, R. Schulz, S. Páll, J.C. Smith, B. Hess, E. Lindahl, Gromacs: High performance molecular simulations through multi-level parallelism from laptops to supercomputers, *SoftwareX* 1–2 (2015) 19–25. <https://doi.org/10.1016/j.softx.2015.06.001>.
- [29] C. Coleman, P.J. van Maaren, M. Hong, J.S. Hub, C.L.T., D. van der Spoel, Force field benchmark of organic liquids: Density, enthalpy of vaporization, heat capacities, surface tension, isothermal compressibility, volumetric expansion coefficient, and dielectric constant, *J. Chem. Theory Comput.* 8 (1) (2012) 61–74. doi: 10.1021/ct200731v.
- [30] V.A. Koverga, O.M. Korsun, O.N. Kalugin, B.A. Marekha, A. Idrissi, A new potential model for acetonitrile: Insight into the local structure organization, *J. Mol. Liq.* 233 (2017) 251–261. <https://doi.org/10.1016/j.molliq.2017.03.025>.
- [31] W.L. Jorgensen, J. Chandrasekhar, J.D. Madura, R.W. Impey, M.L. Klein, Comparison of simple potential functions for simulating liquid water, *J. Chem. Phys.* 79 (2) (1983) 926–935. <https://doi.org/10.1063/1.445869>.
- [32] H.J.C. Berendsen, J.R. Grigera, T.P. Straatsma, The missing term in effective pair potentials, *J. Phys. Chem.* 91 (24) (1987) 6269–6271. <https://doi.org/10.1021/j100308a038>.
- [33] L.-P. Wang, T.J. Martinez, V.S. Pande, Building force fields: An automatic, systematic, and reproducible approach, *J. Phys. Chem. Lett.* 5 (11) (2014) 1885–1891. <https://doi.org/10.1021/jz500737m>.
- [34] D. Vassetzki, M. Pagliai, P. Procacci, Assessment of gaff2 and opls-aa general force fields in combination with the water models tip3p, spce, and op3 for the solvation free energy of druglike organic molecules, *J. Chem. Theory Comput.* 15 (2019) 1983–1995. <https://doi.org/10.1021/acs.jctc.8b01039>.

- [35] M. Parrinello, A. Rahman, Crystal structure and pair potentials: A molecular-dynamics study, *Phys. Rev. Lett.* 45 (1980) 1196–1199, <https://doi.org/10.1103/PhysRevLett.45.1196>.
- [36] W.G. Hoover, Constant-pressure equations of motion, *Phys. Rev. A* 34 (1986) 2499–2500, <https://doi.org/10.1103/PhysRevA.34.2499>.
- [37] G. Martyna, M. Klein, M. Tuckerman, Nosé-hoover chains: The canonical ensemble via continuous dynamics, *J. Chem. Phys.* 97 (4) (1992) 2635–2643, <https://doi.org/10.1063/1.463940>.
- [38] B. Hess, H. Bekker, H. Berendsen, J. Fraaije, Lincs: A linear constraint solver for molecular simulations, *J. Comput. Chem.* 18 (12) (1997) 1463–1472, [https://doi.org/10.1002/\(SICI\)1096-987X\(199709\)18:12<1463::AID-JCC4>3.0.CO;2-H](https://doi.org/10.1002/(SICI)1096-987X(199709)18:12<1463::AID-JCC4>3.0.CO;2-H).
- [39] T. Darden, D. York, L. Pedersen, Particle mesh ewald: An $n \log(n)$ method for ewald sums in large systems, *J. Chem. Phys.* 98 (12) (1993) 10089–10092, <https://doi.org/10.1063/1.464397>.
- [40] W. Humphrey, A. Dalke, K. Schulten, Vmd: Visual molecular dynamics, *J. Mol. Graph. Model.* 14 (1) (1996) 33–38, [https://doi.org/10.1016/0263-7855\(96\)00018-5](https://doi.org/10.1016/0263-7855(96)00018-5).
- [41] M. Brehm, B. Kirchner, Travis - a free analyzer and visualizer for monte carlo and molecular dynamics trajectories, *J. Chem. Inf. Model.* 51 (8) (2011) 2007–2023, <https://doi.org/10.1021/ci200217w>.
- [42] M. Brehm, M. Thomas, S. Gehrke, B. Kirchner, Travis—a free analyzer for trajectories from molecular simulation, *J. Chem. Phys.* 152 (16) (2020) 164105, <https://doi.org/10.1063/5.0005078>.
- [43] C.H. Bennett, Efficient estimation of free energy differences from monte carlo data, *J. Comput. Phys.* 22 (2) (1976) 245–268, [https://doi.org/10.1016/0021-9991\(76\)90078-4](https://doi.org/10.1016/0021-9991(76)90078-4).
- [44] V. Barone, M. Cossi, Quantum calculation of molecular energies and energy gradients in solution by a conductor solvent model, *J. Phys. Chem. A* 102 (11) (1998) 1995–2001, <https://doi.org/10.1021/jp9716997>.
- [45] A. Kulbida, M.N. Ramos, M. Rasanem, J. Nieminen, F. Schrems, O. Rui, Rotational isomerism in acrylic acid. a combined matrix-isolated ir, raman and ab initio molecular orbital study, *J. Chem. Soc., Faraday Trans.* 91 (1995) 1571–1585, <https://doi.org/10.1039/FT9959101571>.
- [46] S.G. Lee, G.F. Brunello, S.S. Jang, J.H. Lee, D.G. Bucknall, Effect of monomeric sequence on mechanical properties of p (vp-co-hema) hydrogels at low hydration, *J. Phys. Chem. B.* 113 (19) (2009) 6604–6612, <https://doi.org/10.1021/jp8058867>.
- [47] D. Sitkoff, K.A. Sharp, B. Honig, Site-specific and sharp, kim a and honig, barry, *The Journal of Physical Chemistry* 98 (7) (1994) 1978–1988, <https://doi.org/10.1021/j100058a043>.
- [48] R. Mills, Self-diffusion in normal and heavy water in the range 1–45. deg., *The Journal of Physical Chemistry* 77 (5) (1973) 685–688, <https://doi.org/10.1021/j100624a025>.
- [49] W.S. Price, H. Ide, Y. Arata, Self-diffusion of supercooled water to 238 k using pgse nmr diffusion measurements, *J. Phys. Chem. A* 103 (4) (1999) 448–450, <https://doi.org/10.1021/jp9839044>.
- [50] W.L. Jorgensen, C. Jenson, Temperature dependence of tip3p, spc, and tip4p water from npt monte carlo simulations: Seeking temperatures of maximum density, *J. Comput. Chem.* 19 (10) (1998) 1179–1186, [https://doi.org/10.1002/\(SICI\)1096-987X\(19980730\)19:10<1179::AID-JCC6>3.0.CO;2-J](https://doi.org/10.1002/(SICI)1096-987X(19980730)19:10<1179::AID-JCC6>3.0.CO;2-J).
- [51] M. Tanaka, G. Girard, R. Davis, A. Peuto, N. Bignell, Recommended table for the density of water between 0 c and 40 c based on recent experimental reports, *Metrologia* 38 (4) (2001) 301, <https://doi.org/10.1088/0026-1394/38/4/3>.
- [52] M. Pagliai, F. Muniz-Miranda, G. Cardini, R. Righini, V. Schettino, Hydrogen bond dynamics of methyl acetate in methanol, *J. Phys. Chem. Lett.* 1 (19) (2010) 2951–2955, <https://doi.org/10.1021/jz1010994>.
- [53] J. Dong, Y. Ozaki, K. Nakashima, Infrared, raman, and near-infrared spectroscopic evidence for the coexistence of various hydrogen-bond forms in poly(acrylic acid), *Macromolecules* 30 (1997) 1111–1117, <https://doi.org/10.1021/ma960693x>.